Journal of Applied Physics

Microscopic and mesoscopic understanding of magnetization compensation phenomenon in ferrimagnetic $Li_{0.5}FeCr_{1.5}O_4$ spinel

Cite as: J. Appl. Phys. **125**, 093903 (2019); https://doi.org/10.1063/1.5064425
Submitted: 04 October 2018 . Accepted: 14 February 2019 . Published Online: 05 March 2019

Madhu Ghanathe, Amit Kumar, and S. M. Yusuf

Journal of Applied Physics ARTICLE scitation.org/journal/jap

Microscopic and mesoscopic understanding of magnetization compensation phenomenon in ferrimagnetic $Li_{0.5}FeCr_{1.5}O_4$ spinel

Cite as: J. Appl. Phys. **125**, 093903 (2019); doi: 10.1063/1.5064425
Submitted: 4 October 2018 · Accepted: 14 February 2019 ·
Published Online: 5 March 2019

Madhu Ghanathe,[1,2] Amit Kumar,[1,2] and S. M. Yusuf[1,2,a)]

AFFILIATIONS

[1]Solid State Physics Division, Bhabha Atomic Research Centre, Mumbai 400085, India
[2]Homi Bhabha National Institute, Anushaktinagar, Mumbai 400094, India

[a)]E-mail: smyusuf@barc.gov.in

ABSTRACT

Structural and magnetic properties of the spinel compound, $Li_{0.5}FeCr_{1.5}O_4$, have been investigated using dc magnetization, neutron depolarization, and neutron diffraction techniques. DC magnetization measurement at 200 Oe has revealed a ferrimagnetic ordering at 417 K and a negative magnetization state between the two compensation temperatures (T_{Comp}) of 244 and 256 K. T_{Comp} varies with an applied magnetic field and two T_{Comp} merge at 256 K for magnetic fields $\geq$ 500 Oe. The existence of zero domain magnetization around T_{Comp} is evident from full recovery of the transmitted neutron beam polarization in a neutron depolarization study. The Rietveld refinement of the neutron diffraction pattern at 430 K reveals that the compound possesses a face centred cubic structure with $Fe_{0.81}Li_{0.19}$ and $Cr_{1.5}Li_{0.31}Fe_{0.19}$ as cation distributions at the tetrahedral and octahedral sites, respectively. A temperature dependent neutron diffraction study reveals that the net magnetic moment changes sign near 265 K, across the spin compensation temperature. Both neutron diffraction and mean field calculation show that an asymmetric variation of the sublattice moments as a function of temperature yields a dominance of the ordered tetrahedral site moment over the octahedral site moment below T_{Comp}, and vice versa above T_{Comp}, and gives a microscopic understanding of the observed magnetization reversal phenomenon. The achieved understanding of magnetization compensation and the high coercivity near T_{Comp} have implications for possible use of such ferrimagnetic materials with finite spin polarization as effective spin polarizers/analyzers in spintronic devices.

I. INTRODUCTION

Several ferrimagnetic materials (below the ferrimagnetic ordering temperature, T_C) show a complete cancellation of net magnetization at a particular temperature known as the compensation temperature (T_{Comp}). In some such materials, a sign change of net magnetization can occur across T_{Comp}, resulting in a negative magnetization phenomenon.[1] This phenomenon was predicted by Louis Néel in spinel ferrites and explained on the basis of the mean field theory.[2] Many ferrimagnetic systems like Co_2VO_4, Co_2TiO_4, Fe_2MoO_4, and $Li_{0.5}Fe_{2.5-x}Cr_xO_4$ spinel compounds, and $R_3Fe_5O_{12}$ garnets (R = Gd, Tb, Dy, Ho, and Eu) exhibit this phenomenon.[1–3] It is postulated that negative magnetization materials hold potential for applications such as spin polarizer/analyzer in spintronic devices.[1] For realization of the application potential, a high compensation temperature (T_{Comp}) around room temperature should be viable in suitable negative magnetization materials. Here, we report our detailed investigation on a $Li_{0.5}FeCr_{1.5}O_4$ spinel compound that has a relatively high T_{Comp} of 282 K under an applied field 50 Oe.

The parent lithium ferrite, $Li_{0.5}Fe_{2.5}O_4$, is a multifunctional material that can have applications in microwave devices, computer memory chips, radio frequency coil fabrication, transformer cores, rod antennas, magnetic liquids, and lithium ion batteries.[4,5] The spinel (AB_2O_4) structure of lithium ferrite can be represented as $Fe^{3+}(A)[Fe^{3+}_{0.75}Li^{1+}_{0.25}\ (B)]_2O^{2-}_4$.[6] The substitution of chromium in place of the Fe^{3+} ion is known to enhance the magnetic properties of lithium ferrite. For example, Gorter *et al.*[7] substituted chromium in place of Fe in the host material to obtain $Li^{1+}_{0.5}Fe^{3+}_{2.5-x}Cr^{3+}_xO^{2-}_4$. The substituted compounds with compositions $1 < x < 1.6$ show a reversal of spontaneous magnetization as a function of temperature.[7] This was further verified by Rais *et al.*[8] The cation distribution for the chromium substituted lithium ferrite was derived from Mössbauer spectroscopy. For $Li^{1+}_{0.5}Fe^{3+}_{2.5-x}Cr^{3+}_xO^{2-}_4$ with $x = 1.25$, the

tetrahedral site (A) contains Fe^{3+} ions and the octahedral site (B) contains $Fe^{3+}/Li^{1+}/Cr^{3+}$, i.e., $(Fe)[Li_{0.5}Cr_{1.25}Fe_{0.25}]O_4$, whereas for $x = 1.55$, the tetrahedral site contains Fe^{3+}/Li^{1+} and the octahedral site contains Li^{1+}/Cr^{3+}, i.e., $(Fe_{0.95}Li_{0.05})[Li_{0.45}Cr_{1.55}]O_4$.[8] The cation distribution, thus, changes with varying substitution and is responsible for the different magnetization behaviours of individual sublattices. However, a detailed experimental microscopic understanding of the reported magnetization reversal for these spinel compounds is lacking in the literature. In this regard, we have taken $x = 1.5$ as an interesting intermediate representative composition, and our study has revealed two magnetization reversals between 229 and 282 K. We have given a very comprehensive physics-oriented understanding of double magnetization reversal in this technologically important system using macroscopic dc magnetization, mesoscopic neutron depolarization, and microscopic neutron diffraction techniques. We mention here that there are conflicting reports on cation distributions for the composition $x = 1.5$. Kuznetsov *et al.*[9] have shown (from the Mössbauer study) that Fe^{3+} ions occupy the tetrahedral site, and Li^{1+} and Cr^{3+} ions occupy the octahedral site, i.e., $(Fe)[Li_{0.5}Cr_{1.5}]O_4$ as a cation distribution, whereas Patil *et al.*[10] (based on the x-ray diffraction study) have shown $(Fe_{0.85}Li_{0.05}Cr_{0.1})[Fe_{0.15}Cr_{1.4}Li_{0.45}]O_4$ as a cation distribution. It is, therefore, important to derive a correct cation distribution for the $x = 1.5$ sample as it is very crucial to understand the magnetization reversal phenomenon. Usually in spinels, the intersublattice [between tetrahedral (A) and octahedral (B) sublattices] exchange interaction is predominant compared with the intrasublattice (tetrahedral-tetrahedral and octahedral-octahedral) exchange interactions. Hence, the cation distributions over the tetrahedral and octahedral sites affect the site magnetic moments and their interactions.[11] Thus, in the present work using the powerful neutron diffraction technique, the ambiguity in the cation distribution is resolved, and a microscopic understanding on negative magnetization has been obtained by measuring the temperature dependent site magnetic moments.[12] The behaviour of domain magnetization in the vicinity of magnetization reversal in a mesoscopic length scale has also been studied by employing the neutron depolarization technique. Interestingly, we have observed a high coercivity around T_{Comp} with negligible remanent magnetization. The gained knowledge of magnetization compensation and high coercivity near T_{Comp} have implications for possible use of such ferrimagnetic materials with finite spin polarization as effective spin polarizers/analyzers in spintronic devices.

II. EXPERIMENTAL DETAILS

The polycrystalline compound $Li_{0.5}FeCr_{1.5}O_4$ was synthesized by the standard double sintering ceramic technique. Stoichiometric mixtures of high purity (>99.9%) oxides Fe_2O_3, and Cr_2O_3, and carbonate Li_2CO_3 were thoroughly mixed for 1 h in an agate mortar with a pestle. The homogeneous mixture of the compounds was compressed using a unidirectional hydraulic press at 4 tons to form pellets. The pellets were calcinated in air at 1000 °C for 12 h and then cooled down to room temperature, ground manually, and pelletized again. The final sintering was done at 1200 °C for 12 h in a furnace.[8] An X-ray diffraction study was carried out at room temperature using a CuK_α radiation. The X-ray diffraction pattern was recorded with a step size of 0.02° over a scattering angular (2θ) range of 10°-80°. In order to study the detailed crystal and magnetic structures of the compound, neutron-diffraction data were recorded over a temperature range of 7–430 K using the powder diffractometer-I (PD-I) and the powder diffractometer-II (PD-II) at Dhruva reactor, Trombay, India. PD-I operates at a wavelength of 1.094 Å using a single crystal Si (422 Bragg reflection) monochromator and position sensitive detectors that cover a scattering angle up to 70° with a resolution ($\Delta d/d$) of ~1%. PD-II operates at a wavelength of 1.2443 Å using a single crystal Ge (331 Bragg reflection) monochromator and five position sensitive detectors covering a scattering angle up to 140° with a resolution ($\Delta d/d$) of ~0.8%. Rietveld refinements of neutron diffraction patterns were carried out using the FULLPROF computer program.[13] The dc magnetization (M) measurements were carried out on the compound using a Physical Property Measurement System (PPMS) as a function of temperature (T) and magnetic field (H). The magnetization vs. temperature measurements were carried out over a temperature range of 5–570 K. However, it is important to describe the modes of dc magnetization measurements under various thermal cycles. In the field-cooled cooling mode (FCC), measurements were carried out in the presence of an external magnetic field in the cooling cycle itself. Field-cooled warming (FCW) curves were obtained by first cooling the sample in the presence of the magnetic field and then measurements were carried out in a warming cycle with the applied magnetic field "ON." A small and positive magnetic field of 3 Oe was achieved at the PPMS by using the following procedure. First, the remanent magnetic field of the superconducting magnet was brought down below 10 Oe by carrying out the standard degaussing procedure. Further, a standard sample of Nb of known magnetization was loaded using the low-field measurement probe of the PPMS under its low-field option. The field of the magnet was reduced to the order of 3 Oe by lowering the applied current to the magnet to match the magnetization of the standard sample of Nb with its reported value. This ensured a very low positive field of 3 Oe. By keeping the same field on, the $Li_{0.5}FeCr_{1.5}O_4$ sample was measured in the FCW mode. The one dimensional neutron depolarization measurement over a temperature range of 5–300 K (in FCW cycle) was carried out using the polarized neutron spectrometer ($\lambda = 1.201$ Å) at Dhruva reactor, Trombay, Mumbai, India.[14] The monochromator-cum-polarizer Cu_2MnAl (111) single crystal (polarization efficiency ~ 98.8%) was used to polarize the incident neutron beam in the –z (vertically down) direction. To analyze the transmitted neutron beam polarization, we used $Co_{0.92}Fe_{0.08}$ (200) single crystal as an analyser (efficiency ~ 97.4%).

III. RESULTS AND DISCUSSION

A. X-ray diffraction

Single phase crystalline nature of the compound was confirmed by the x-ray diffraction technique (Fig. 1). The main reflections (hkl) of the spinel structure of the ferrite are identified in the x-ray diffraction pattern of $Li_{0.5}FeCr_{1.5}O_4$ as (111), (220), (311), (400), (422), (511), and (440).[15] In $Li_{0.5}FeCr_{1.5}O_4$, x-ray is unable to detect Li (due to low atomic number) and differentiate between Fe and Cr (due to nearly the same atomic numbers) cations in the sample. Therefore, the neutron diffraction technique is employed to gain

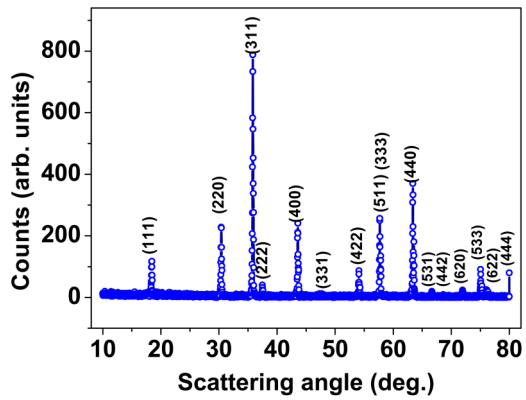

FIG. 1. X-ray diffraction pattern of $Li_{0.5}FeCr_{1.5}O_4$ with hkl values of the peaks.

information about precise cation distribution over two crystallographic sites in the sample.

B. DC magnetization

Figure 2(a) shows FCC M vs T curve under an applied magnetic field of 200 Oe for $Li_{0.5}FeCr_{1.5}O_4$ over a temperature range of 570–5 K. The compound shows a magnetic ordering (T_C) at 417 K, obtained by the method of "intersecting tangents."[8] The temperature dependent magnetization increases below T_C, meanwhile after reaching 350 K, magnetization becomes almost constant, and then decreases below 350 K and vanishes around 256 K. This temperature (256 K) is known as the compensation temperature (T_{Comp}). The magnetization then remains slightly negative until the descending temperature reaches at a value of 244 K. Finally, below 244 K, the magnetization becomes positive again with a large growth. In order to gain more insight into the compensation phenomenon, we depict the FCC and the FCW M vs T curves under various applied magnetic fields for the compound over the limited temperature range of 5–310 K in Fig. 2(b). It is seen that for a negligibly small (~3 Oe) magnetic field, the magnetization compensation occurs only once at ~265 K and magnetization remains negative below this temperature. However, for 10 Oe $\lesssim H <$ 500 Oe, negative magnetization appears only over the temperature range of 229 to 282 K [Fig. 2(c)], providing two compensation temperatures. Out of the two compensation temperatures, one compensation temperature (256 K) is field independent in both FCC and FCW cases. However, the other compensation temperature is very much field dependent and shows different behaviour in FCC and FCW cases as shown in Fig. 2(d). As the applied external magnetic field for the FCC and FCW measurements increases, the temperature gap between the two compensation temperatures decreases and at an applied field of 500 Oe, the two compensation temperatures get merged to 256 K, which is close to the value of T_{Comp} (=253 K) reported by Pauleve *et al.*[16]

The M vs H data have been recorded at various temperatures and under magnetic fields up to 60 kOe, and are shown in Fig. 3(a).

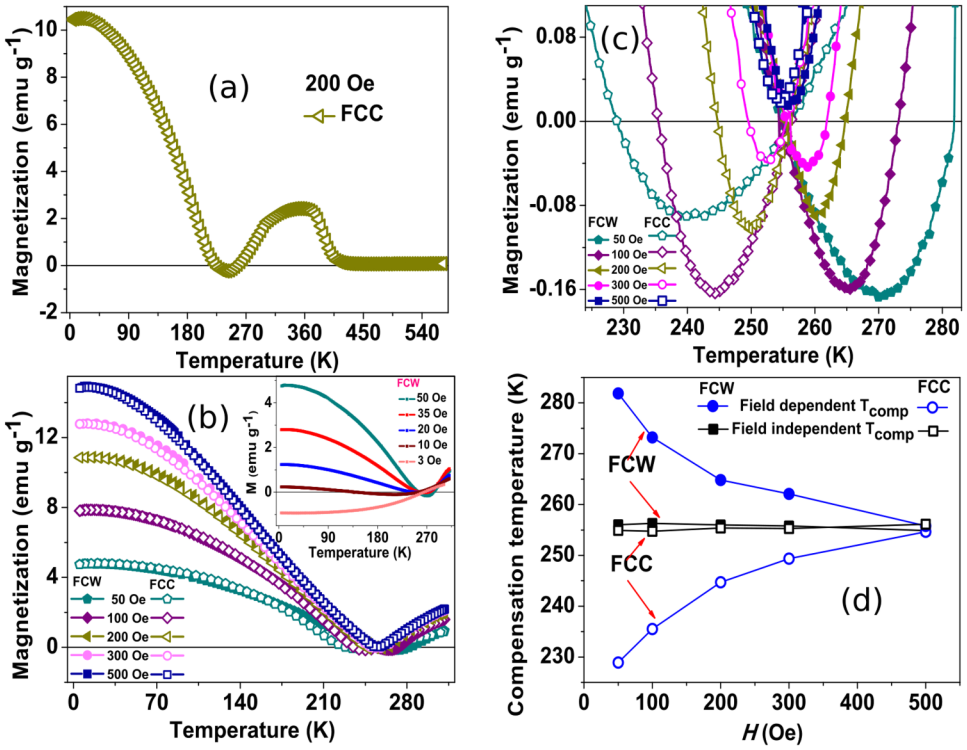

FIG. 2. (a) Temperature dependent FCC dc magnetization under 200 Oe. (b) Temperature dependent FCC and FCW dc magnetization curves under various applied fields. Inset shows temperature dependent FCW magnetization curves under smaller applied fields of 50, 35, 20, 10, and 3 Oe. (c) Enlarged view of temperature dependent crossover of FCC and FCW magnetizations from positive to negative value. (d) Variations of field dependent and field independent compensation temperatures in both FCC and FCW modes of magnetization measurements at various applied magnetic fields. Lines connecting the data points are a guide to the eyes.

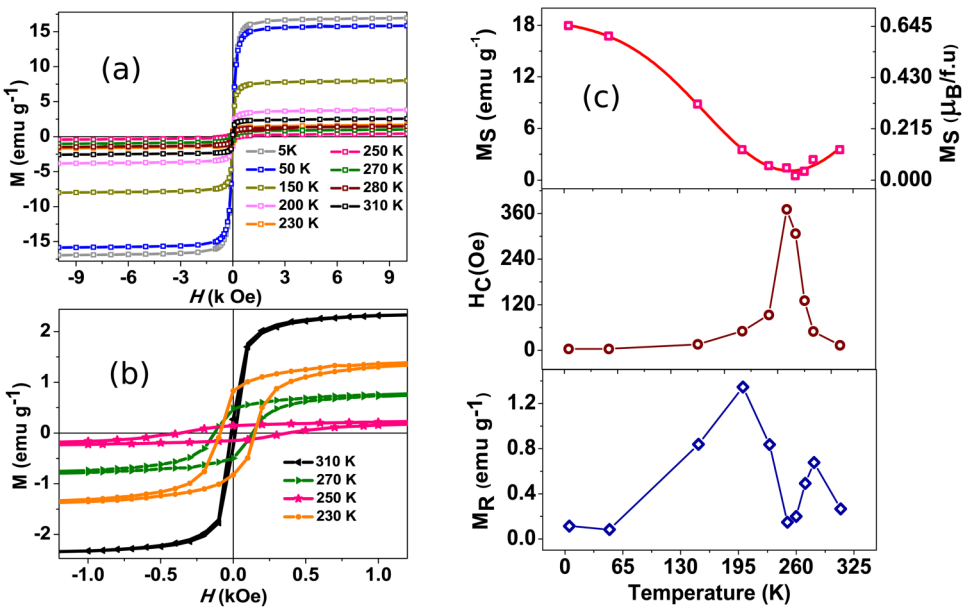

FIG. 3. (a) Hysteresis curves at various temperatures. (b) Enlarged view of hysteresis curves. (c) Variation of saturation magnetization (M_S), coercive field (H_C), and remanent magnetization (M_R) with temperature. Lines connecting the data points are visual guides.

An enlarged view of the hysteresis curves at low fields is depicted in Fig. 3(b). Temperature variations of saturation magnetization (M_S), coercive field (H_C), and remanent magnetization (M_R), derived from the hysteresis curves, are plotted in Fig. 3(c). Saturation magnetization is another parameter that reveals the presence of magnetization compensation at T_{Comp}. It is observed that, at $T < T_{Comp}$, the saturation magnetization decreases with increasing temperature, showing a minimum (negligible value) near T_{Comp}. However, just above T_{Comp}, it increases with increasing temperature. Significantly, an increase in the H_C near the compensation temperature indicates that the H_C is inversely proportional to the M_S (as per Stoner-Wohlfarth model,[17] $H_C = 2K/M_S$, where K is the anisotropic constant). Similar behaviour has been found in rare earth iron garnets, where single or double peak of coercivity near T_{Comp} suggests the growth of coercivity with decreasing magnetization. M_R also shows an anomalous variation with temperature around T_{Comp}. This kind of variation of M_R is probably a consequence of anomalous variations of M_S and H_C across T_{Comp}. The observed high H_C around T_{Comp} is due to the negligible M_R. Here, a relatively higher external magnetic field is essential to demagnetize the sample (i.e., higher H_C) as the effective coupling between applied field and M_R is quite weak for vanishingly small M_R. Interestingly, this ferrimagnetic material at T_{Comp} possesses a finite spin polarization but zero magnetization with high coercivity that opens up the possibility of applications in spintronic devices[1,3] as discussed later.

C. Neutron depolarization

In order to gain further understanding of the observed negative magnetization for this compound, we have carried out a detailed temperature dependent neutron depolarization study. This technique can provide information of domain magnetization and its size variation with temperature on a mesoscopic length scale.[18–20] This is achieved by polarized neutrons, transmitted through the unsaturated ferrimagnetic system, causing the Larmor precession of neutron spin under local magnetic induction of domains and resulting in depolarization of the transmitted neutron beam.[14,21] Here, we remind that magnetically disordered systems, such as paramagnets and spin-glasses, have no effect on polarisation.[22–24] The expression for the neutron beam polarization in a depolarization experiment can be written as

$$P_f = P_i \exp\left[-\alpha\left(\frac{d}{\delta}\right)\langle\Phi_\delta\rangle^2\right]. \quad (1)$$

In the above mentioned Eq. (1), transmitted neutron beam polarization P_f depends on the initial neutron beam polarization (P_i), dimensionless parameter ($\alpha \sim 1/3$), effective sample thickness d, average domain size (δ), and average precession angle over a magnetic domain $\langle\Phi_\delta\rangle = (4.63 \times 10^{-10}\,\mathrm{G^{-1}\,\AA^{-2}})\lambda\delta B_0$. Here, λ (in Å) is the wavelength of the neutron beam and B_0 (in Gauss) is the average magnetic induction of the domain ($B_0 = 4\pi M_{sp}\rho$ where, M_{sp} is spontaneous magnetization in emu/g, and ρ is the density of the sample in g/cm^3). Here, M_{sp} value can be extracted from dc magnetization hysteresis curves. The above equation is valid only when the precession angle over a domain length is a small fraction of 2π and is applicable for the present case.[25,26]

Figure 4 depicts the neutron depolarization curves for the compound measured under 50 Oe field in FCC and FCW modes. Transmitted neutron beam is depolarized at 300 K due to the magnetization of the finite size domains. An average magnetic induction of the domain ($B_0 = 81$ Gauss) is obtained by using average sample density 4.71 g cm^{-3} and the observed spontaneous magnetization 3.5 emu g^{-1} at 300 K in Fig. 3. The average precession angle

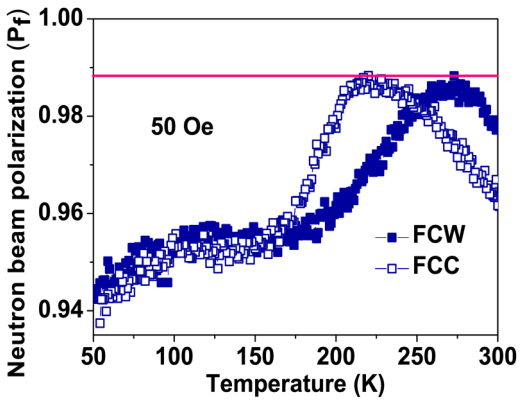

FIG. 4. Transmitted neutron beam polarization curves under 50 Oe in FCC and FCW modes for $Li_{0.5}FeCr_{1.5}O_4$ compound. The red horizontal line corresponds to the incident neutron beam polarization.

$\langle\Phi_\delta\rangle$ is calculated in terms of average domain size δ using wavelength of the beam 1.201 Å. Substituting all required values in Eq. (1), an average magnetic domain size, $\delta = 10\,\mu m$ is obtained at 300 K. However, neutron beam polarization recovers completely (same as the incident beam polarization) around 274 and 224 K in the FCW and FCC modes, respectively, confirming the presence of irreversibility between two modes with two T_{Comp} values as found in our dc magnetization study (Fig. 2). Full recovery of polarization indicates that magnetization of the domains is zero due to spin compensation inside each magnetic domain in $Li_{0.5}FeCr_{1.5}O_4$.[3] Below T_{Comp}, neutron beam depolarization again increases due to finite domain magnetization. The behaviour of depolarization curves in both FCC and FCW modes is in good agreement with the dc magnetization curve (50 Oe) shown in Fig. 2(c).

D. Neutron diffraction

In order to gain a microscopic understanding of the observed negative magnetization for the present system, we have carried out a detailed temperature dependent neutron diffraction study. Figure 5 shows the Rietveld refined neutron-diffraction patterns for the sample at various temperatures (7–430 K). The Rietveld refinement of the neutron diffraction pattern at 430 K (paramagnetic phase) confirms that the sample is in single phase having a face centred cubic (fcc) crystal structure with space group $Fd\bar{3}m$ (No. 227) as reported in the literature.[15] The chemical unit cell consists of 8 $Li_{0.5}FeCr_{1.5}O_4$ formula units. The 32 oxygen ions form an fcc structure with an edge length of 8.2918(1) Å [Fig. 6(a)].

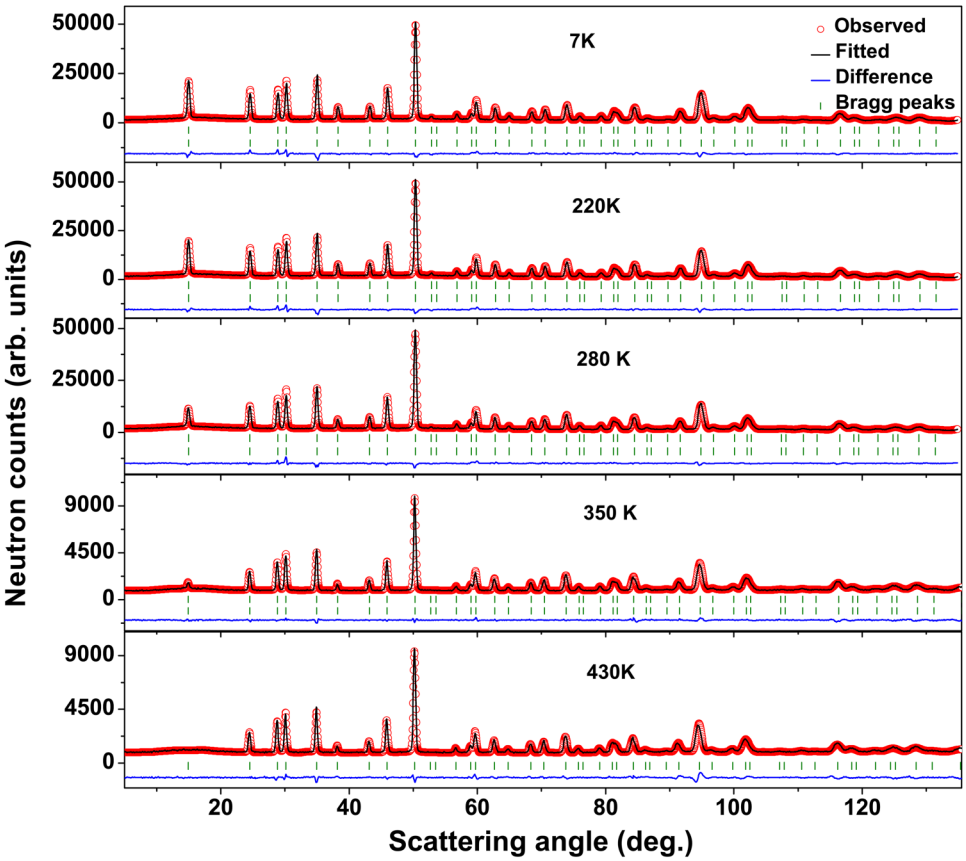

FIG. 5. Rietveld refined neutron diffraction patterns at various temperatures for $Li_{0.5}FeCr_{1.5}O_4$. The open circle and the solid line represent the observed and fitted patterns, respectively, and the difference between observed and fitted patterns is plotted at the bottom of each view graph. The short vertical lines (upper and lower) represent the positions of (nuclear and magnetic) Bragg peaks. The pattern at 430 K is fitted only with the nuclear phase.

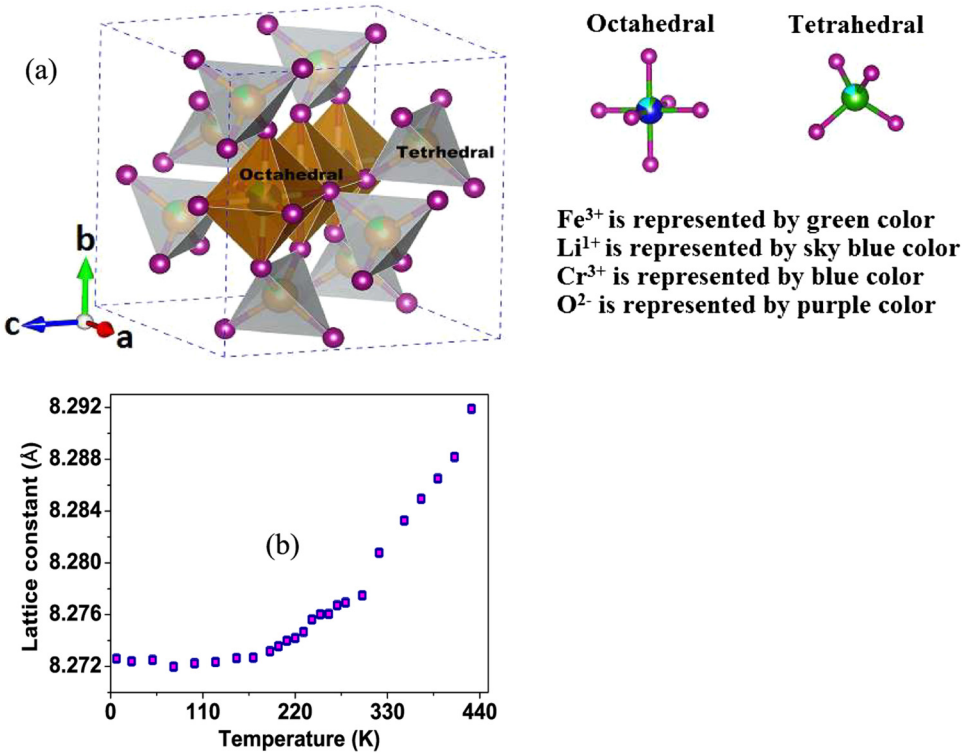

FIG. 6. (a) Schematic view of the spinel structure of $Li_{0.5}FeCr_{1.5}O_4$ compound with octahedral and tetrahedral units. (b) Variation of the lattice constant with temperature.

The change in edge length of unit cell with temperature is shown in Fig. 6(b). The compound possesses a single phase mixed spinel structure where Fe^{3+}/ Li^{1+} cations occupy the 8a (1/8, 1/8, 1/8) site (A sublattice) under the tetrahedral O^{2-} coordination environment, and $Fe^{3+}/Cr^{3+}/Li^{1+}$ cations occupy the 16d (1/2, 1/2, 1/2) site (B sublattice) under the octahedral O^{2-} coordination environment. Here, we would like to mention that the (220), (400), and (440) Bragg peaks are quite sensitive to the site occupancies of cations.[12,27] Cation distribution and other structural parameters derived from the Rietveld refinement are represented in Table I. The derived cation distribution can be represented as $(Fe_{0.81}Li_{0.19})[Cr_{1.5}Li_{0.31}Fe_{0.19}]O_4$.

TABLE I. Structural parameters for $Li_{0.5}FeCr_{1.5}O_4$ at 430 K. R_p: 2.52%; R_{wp}: 3.43%; R_{exp}: 2.98%; tet: Tetrahedral site; oct: Octahedral site; and B: Isotropic temperature factor.

Space group = Fd$\bar{3}$m, a = 8.2918(1) (Å)					
Atoms	x	y	z	**Occupancy**	**B (Å^2)**
Fe (tet)	0.125	0.125	0.125	0.81(1)	0.9(3)
Li (tet)	0.125	0.125	0.125	0.19(1)	0.9(3)
Fe (oct)	0.5	0.5	0.5	0.19(1)	0.5(3)
Li (oct)	0.5	0.5	0.5	0.31(1)	0.5(3)
Cr (oct)	0.5	0.5	0.5	1.50	0.5(3)
O	0.2586(4)	0.2586(4)	0.2586(4)	4	0.9(2)

Neutron diffraction patterns, collected at various temperatures below the magnetic ordering temperature (T_C = 417 K) (Fig. 5), show that the intensity of the (111) Bragg peak rises rapidly with lowering of temperature and provides information on the magnetic structure of the system. The temperature variations of intensities of nuclear cum magnetic Bragg peaks, viz., (220) and (222), represent the growth of the ordered magnetic moments M_T and M_O at the tetrahedral and octahedral sites, respectively.[3,28] The net ordered magnetic moment (M_{Net}) per formula unit (AB_2O_4) of the system, $Li_{0.5}FeCr_{1.5}O_4$ is derived using $M_{Net} = 2|M_O| - |M_T|$. Thermal variations of ordered magnetic moments (M_T, M_O, and M_{Net}) under zero applied field are depicted in Fig. 7(a). The temperature dependent net magnetic moment of the system increases below the ordering temperature, takes a down turn at 350 K and becomes zero at 265 K (T_{Comp}), and remains negative below T_{Comp}. Here, we would like to mention that since the neutron diffraction measurements are carried out under zero field, only one compensation temperature (consistent with the dc magnetization data under 3 Oe) is observed against two compensation temperatures in FCC and FCW modes of dc magnetization for 10 Oe $\lesssim H <$ 500 Oe. Further, the presence of a single compensation temperature in dc magnetization curves under $H \geq$ 500 Oe indicates that two T_{Comp} are linked to the ferrimagnetic domain behaviour under different cooling conditions for this ferrimagnetic system.[29,30] The presence of moment compensation in Fig. 7 indicates anomaly in the growth of magnetic moments for the sublattices above and below T_{Comp}. A molecular field theory (MFT) calculation has been done to explain the

observed negative magnetization phenomenon with a two sublattice model. The adopted MFT theory has been explained in detail in the next paragraph. The magnetic exchange interaction between the ions placed at *A* and *B* sites is negative. This strong negative exchange interaction makes the magnetic moments of the A site ions align themselves opposite to the direction of alignment of magnetic moments of the B site ions.[31,32] Figure 7(b) shows the schematic of the magnetic unit cell showing antiparallel orientation of magnetic moments of the two sites at $T < T_{Comp}$ in the absence of an external magnetic field. Figure 7(c) represents the growth of sublattice magnetic moments and net magnetization (M_{Domain}) inside a ferrimagnetic domain (pictorially represented as efgh) above and below T_{Comp}, as extracted from our neutron diffraction study under zero magnetic field. The magnetic moment of the net octahedral sublattice in a formula unit ($= 2M_O$) dominates over that of tetrahedral sublattice ($= M_T$) above T_{Comp} and vice-versa below T_{Comp}, resulting in a sign reversal of the M_{Net} (as well as of M_{Domain}). However, a different behaviour is observed in a dc magnetization study under an external magnetic field below $T < T_{Comp}$ (Fig. 2). In the case of the observed dc magnetization curve under 500 Oe field [Fig. 2(b)], a competition between anisotropic energy and Zeeman energy (applied magnetic field) is evident. The Zeeman energy overtakes the anisotropic energy and rotates the direction of the net magnetization of the domain [shown as ghef in Fig. 7(d)] in the direction of applied magnetic field below T_{Comp}, so that the net magnetization under a magnetic field (500 Oe) remains positive down to 5 K. Recalling the cation distribution $(Fe_{0.81}Li_{0.19})[Cr_{1.5}Li_{0.31}Fe_{0.19}]O_4$ in $Li_{0.5}FeCr_{1.5}O_4$, the presence of higher percentage of non-magnetic ions Li^{1+} on the tetrahedral site contributes to a sharper fall in the A site magnetic moment with increasing temperature above T_{Comp}. This leads to the dominance of *B* site magnetic moment over *A* site magnetic moment in the 260–417 K range.

E. Mean field calculation

The theoretical investigation of two sublattice magnetization has been carried out under the formalism of the Néel theory of ferrimagnetism.[2] The magnetic moments of tetrahedral (*T*) and

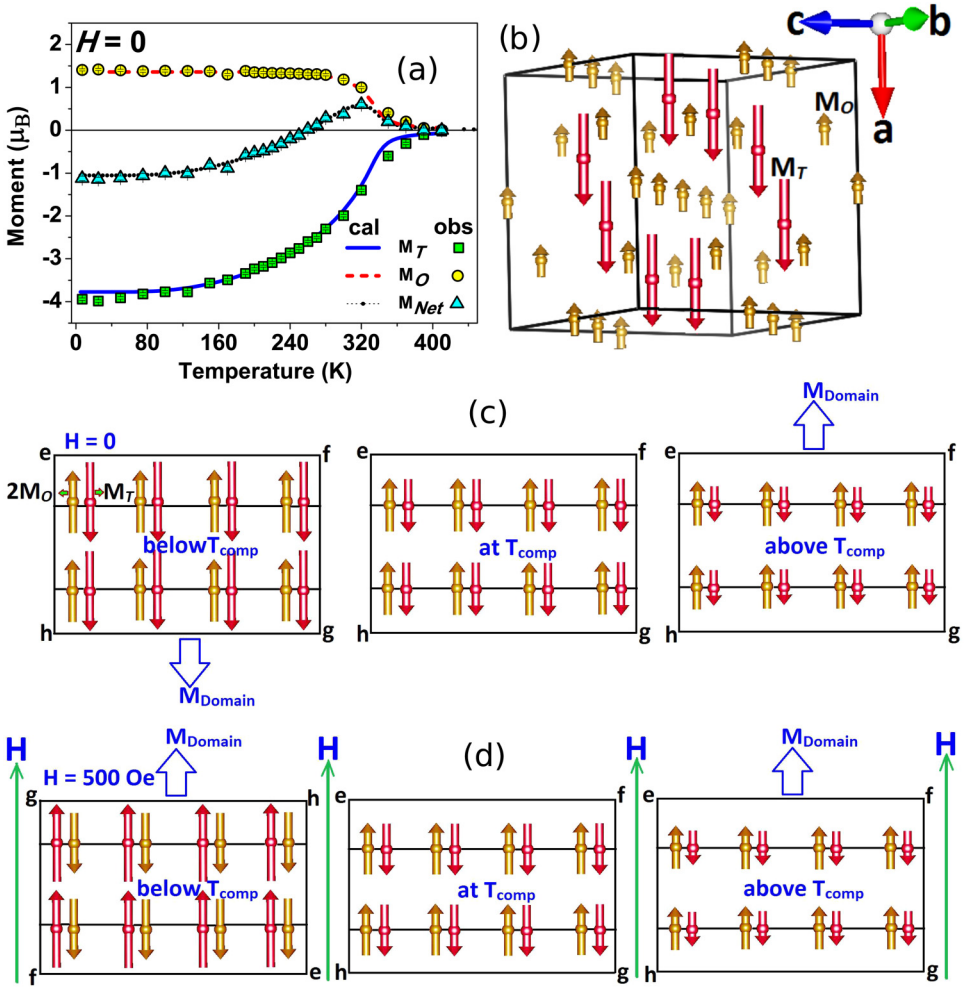

FIG. 7. (a) Thermal variations of ordered magnetic moments of tetrahedral site (M_T), octahedral site (M_O), and net magnetic moment per formula unit (M_{Net}) extracted from the Rietveld refined neutron diffraction patterns measured under zero external magnetic field (symbols: observed values). The error bars are smaller than the size of the symbols. Lines represent the calculated values of magnetic moments based on the molecular field theory. (b) Schematic view of the magnetic unit cell showing relative orientations of the octahedral and tetrahedral site moments at $T < T_{Comp}$ under zero applied magnetic field. (c) and (d) The pink {yellow} color vectors represent the variation of direction and magnitude of tetrahedral (M_T) {octahedral ($2M_O$)} sublattice magnetic moments inside a magnetic domain (efgh) at three different temperature regions in the presence and absence of an external magnetic field as inferred from (c) neutron diffraction and (d) dc magnetization data. ghef represents the rotation of magnetic domains through 180° in the presence of an applied field of 500 Oe. The direction of the net magnetization of the domain (M_{Domain}) is represented as the blue color arrow mark in (c) and (d).

octahedral sites (O) are represented by M_T and M_O, respectively. The antiferromagnetic interaction between these two sublattices results in a net magnetization of the spinel (AB_2O_4) compound, represented as $M_{Net} = 2|M_O| - |M_T|$.[33]

Referring to the MFT, $M_i = N_i\ S_i\ g_i\ \mu_B\ B(y_i)$. Here, M_i is the magnetization of the ith sublattice ($i = T$ and O), N_i is the number of magnetic ions per unit volume, S_i is the average spin angular momentum, g_i represents the Lande-g factor, μ_B is the Bohr magneton, and the Brillouin function is expressed as

$$B(y_i) = [(2S_i + 1)/2S_i]\coth\{[(2S_i + 1)/2S_i].y_i\} - (1/2S_i)\coth[(1/2S_i).y_i], \quad (2)$$

where

$$y_i = S_i g_i \mu_B H_i / K_B T. \quad (3)$$

In terms of the MFT, molecular fields at the tetrahedral and octahedral sublattices (H_T and H_o) can be expressed as

$$\left.\begin{aligned} H_T &= H_e + \lambda_{T-T}M_T + \lambda_{T-O}M_O \\ H_O &= H_e + \lambda_{O-T}M_T + \lambda_{O-O}M_O \end{aligned}\right\}, \quad (4)$$

where $\lambda_{T\text{-}T}$ and $\lambda_{O\text{-}O}$ denote the intra-sublattice molecular field coefficients, $\lambda_{T\text{-}O}$ and $\lambda_{O\text{-}T}$ denote the inter-sublattice molecular field coefficients, and H_e is the externally applied magnetic field.

The inter-sublattice interaction is mediated by oxygen atoms. The super exchange interaction (J) between inter-sublattices is stronger than the intra-sublattice interactions. Therefore, $\lambda_{T\text{-}T}$ and $\lambda_{O\text{-}O}$ are neglected in the present case. The molecular field coefficients for inter sublattice interactions are written as

$$\left.\begin{aligned} \lambda_{T-O} &= (2Z_{T-O}J)(2.5 - x)/[y_T N_T (g\mu_B)^2] \\ \lambda_{O-T} &= (2Z_{O-T}J)(x)/[y_O N_O (g\mu_B)^2] \end{aligned}\right\}, \quad (5)$$

where $Z_{T\text{-}O}$ ($Z_{O\text{-}T}$) is the number of octahedral (tetrahedral) ions surrounded by tetrahedral (octahedral) ions. The $\lambda_{T\text{-}O}$ and $\lambda_{O\text{-}T}$ are derived as per the formula unit of $Li_{0.5}Fe_{2.5-x}Cr_xO_4$ for $x = 1.5$ composition. The strength of the super exchange interaction (J) is derived from the observed magnetic ordering temperature ($T_C = 417$ K) of the compound[34]

$$|J| = 3K_B T_C/2.\left[(Z_{T-O}Z_{O-T})S_T(S_T + 1)S_O(S_O + 1)\right]^{1/2}. \quad (6)$$

The presence of non-magnetic lithium ions on both tetrahedral (T) and octahedral (O) sites affects the average spin on both sites; therefore, considering the cation distribution obtained from neutron diffraction study, spin values of $S_T = 1.25$ and $S_O = 0.75$ have been taken for the calculation of J and sublattice magnetization. The super exchange interaction strength $|J| = 4.1 \times 10^{-22}$ J is obtained using the values $Z_{T\text{-}O} = 12$, and $Z_{O\text{-}T} = 6$.[35] Substituting all the relevant values, magnetic moments of both tetrahedral and octahedral sublattices are calculated as a function of temperature under zero external field. The net ordered magnetic moment (M_{Net}) per formula unit (AB_2O_4) of the system, $Li_{0.5}FeCr_{1.5}O_4$ is calculated as $M_{Net} = 2|M_O| - |M_T|$. Comparison between the calculated magnetic moment and the observed magnetic moment from neutron diffraction experiments provides a satisfactory agreement as shown in Fig. 7(a).

Now, we briefly discuss the application potential of such a spin compensated ferrimagnetic material. The present ferrimagnetic material at T_{Comp} possesses a finite spin polarization[36] which would be unaffected by the external electromagnetic fields due to zero magnetization (Fig. 2) as well as a large coercivity (Fig. 3). This opens up the possibility of using such ferrimagnetic materials as effective spin polarizers/analyzers in spintronic devices.[37] Further, such a material, through interfacial magnetic coupling,[38] could be utilized to flip (by varying the temperature across T_{Comp}) the magnetization of an adjacent ferromagnetic layer in a spin transfer torque based magnetic random access memory (STT-MRAM) device.[3]

IV. SUMMARY AND CONCLUSIONS

We have studied the magnetization reversal phenomenon in high Curie temperature spinel ferrite, $Li_{0.5}FeCr_{1.5}O_4$, on macroscopic, mesoscopic, and microscopic length scales. The results obtained through various measurements, such as dc magnetization, neutron diffraction, and neutron depolarization, provide indisputable evidence of the magnetization reversal leading to negative magnetization in this spinel system. Magnetic ordering sets in at 417 K with a compensation temperature of 256 K. Furthermore, the neutron diffraction study infers a disordered *fcc* crystal structure with $(Fe_{0.83}Li_{0.17})[Cr_{1.5}Li_{0.33}Fe_{0.17}]O_4$ as the cation distribution. The antiferromagnetic exchange interaction between the tetrahedral and the octahedral sublattices favours the compensation of magnetization due to the cancellation of oppositely aligned magnetic moments of the two sublattices. This has been further established by the neutron depolarization study, where a full recovery of neutron beam polarization around T_{Comp} confirms a zero domain magnetization state. The temperature dependent neutron diffraction study reveals that the net magnetic moment changes sign from positive to negative at 265 K with decreasing temperature. The experimental results have been supported by a mean field calculation. The present study also concludes an asymmetric variation of the sublattice moments resulting in dominance of the ordered tetrahedral site moment (M_T) over the octahedral site moment (M_O) below T_{Comp} and vice versa above T_{Comp}. A large coercivity near T_{Comp} opens up the possibility of using such ferrimagnetic materials with finite spin polarization as effective spin polarizers/analyzers in spintronic devices.

ACKNOWLEDGMENTS

M.G. would like to thank the Department of Science and Technology, India (DST), for support through the Inspire fellowship of AORC programme of DST, India.

References

[1] A. Kumar and S. M. Yusuf, Phys. Rep. **556**, 1 (2015).
[2] J. S. Smart, Am. J. Phys. **23**, 356 (1955).
[3] A. Kumar and S. M. Yusuf, J. Appl. Phys. **121**, 223903 (2017).

[4]G. Wei, L. Wei, D. Wang, Y. Chen, Y. Tian, S. Yan, L. Mei, and J. Jiao, Sci. Rep. **7**, 12554 (2017).
[5]R. G. West and A. C. Blankenship, J. Am. Ceram. Soc. **50**, 343 (1967).
[6]S. Sílvia, M. Graça, M. Valente, and L. Costa, *Lithium Ferrite: Synthesis, Structural Characterization and Electromagnetic Properties* (IntechOpen, 2017).
[7]E. W. Gorter and J. A. Schulkes, Phys. Rev. **90**, 487 (1953).
[8]A. Rais, A. M. Gismelseed, and I. A. Al-Omari, Phys. Status Solid. (b) **242**, 2949 (2005).
[9]M. V. Kuznetsov, Q. A. Pankhurst, and I. P. Parkin, J. Phys. D Appl. Phys. **31**, 2886 (1998).
[10]R. P. Patil, A. D. Pinjarkar, D. J. Sathe, A. S. Chavan, S. D. Delekar, and P. P. Hankare, J. Mater. Sci. Mater. Electron. **27**, 1574 (2016).
[11]E. W. Gorter, Philips Res. Rep. **9**, 295 (1954).
[12]S. M. Yusuf and A. Kumar, Appl. Phys. Rev. **4**, 031303 (2017).
[13]R. J. Hill and C. J. Howard, J. Appl. Crystallogr. **20**, 467 (1987).
[14]S. M. Yusuf and L. M. Rao, Neutron News **8**, 12 (1997).
[15]L. Fernández-Barquín, M. V. Kuznetsov, Y. G. Morozov, Q. A. Pankhurst, and I. P. Parkin, Int. J. Inorg. Mater. **1**, 311 (1999).
[16]J. Pauleve, J. Appl. Phys. **29**, 259 (1958).
[17]S.-I. Ohkoshi, T. Iyoda, A. Fujishima, and K. Hashimoto, Phys. Rev. B **56**, 11642 (1997).
[18]S. M. Yusuf, M. Sahana, M. S. Hegde, K. Dörr, and K.-H. Müller, Phys. Rev. B **62**, 1118 (2000).
[19]J. M. De Teresa, C. Ritter, P. A. Algarabel, S. M. Yusuf, J. Blasco, A. Kumar, C. Marquina, and M. R. Ibarra, Phys. Rev. B **74**, 224442 (2006).
[20]S. M. Yusuf, K. R. Chakraborty, S. K. Paranjpe, R. Ganguly, P. K. Mishra, J. V. Yakhmi, and V. C. Sahni, Phys. Rev. B **68**, 104421 (2003).
[21]S. M. Yusuf, K. R. Chakraborty, A. Kumar, A. Jain, V. Siruguri, and P. D. Babu, Neutron News **25**, 22 (2014).
[22]O. Halpern and T. Holstein, Phys. Rev. **59**, 960 (1941).
[23]S. Mitsuda, H. Yoshizawa, and Y. Endoh, Phys. Rev. B **45**, 9788 (1992).
[24]S. M. Yusuf and L. M. Rao, Pramana, J. Phys. **47**, 171 (1996).
[25]A. Kumar and S. M. Yusuf, Physica B **551**, 104 (2018).
[26]S. M. Yusuf, M. Sahana, K. Dörr, U. K. Rößler, and K.-H. Müller, Phys. Rev. B **66**, 064414 (2002).
[27]G. O. White and C. E. Patton, J. Magn. Magn. Mater. **9**, 299 (1978).
[28]R. Chakravarthy, L. Madhav Rao, S. K. Paranjpe, S. K. Kulshreshtha, and S. B. Roy, Phys. Rev. B Condens. Matter **43**, 6031 (1991).
[29]A. Kumar, S. M. Yusuf, and L. Keller, Phys. Rev. B **71**, 054414 (2005).
[30]S. M. Yusuf and L. M. Rao, J. Phys. Condens. Matter **7**, 5891 (1995).
[31]K. P. Belov, Phys. Usp. **39**, 623 (1996).
[32]Y. Yafet and C. Kittel, Phys. Rev. **87**, 290 (1952).
[33]C. M. Srivastava, G. Srinivasan, and N. G. Nanadikar, Phys. Rev. B **19**, 499 (1979).
[34]S. M. Yusuf, A. Kumar, and J. V. Yakhmi, Appl. Phys. Lett. **95**, 182506 (2009).
[35]Y.-P. Fu, Mater. Chem. Phys. **115**, 334 (2009).
[36]P. V. Lukashev, J. D. Burton, A. Smogunov, J. P. Velev, and E. Y. Tsymbal, Phys. Rev. B **88**, 134430 (2013).
[37]H. Adachi and H. Ino, Nature **401**, 148 (1999).
[38]P. K. Manna and S. M. Yusuf, Phys. Rep. **535**, 61 (2014).